Journal of Morphology

WILEY

JOURNAL OF morphology

RESEARCH ARTICLE

Functional Divergence of Scorpion Pedipalps: Musculoskeletal Specialization Toward Opposing Performance Optima

Yuri Simone[1,2,3] | Anthony Herrel[3,4,5,6] | Renaud Boistel[4] | Arie van der Meijden[1,2]

[1]CIBIO, Centro de Investigação em Biodiversidade e Recursos Genéticos, InBIO Laboratório Associado, Campus de Vairão, Universidade do Porto, Vairão, Portugal | [2]BIOPOLIS Program in Genomics, Biodiversity and Land Planning, CIBIO, Campus de Vairão, Vairão, Portugal | [3]Department of Biology, University of Antwerp, Wilrijk, Belgium | [4]UMR 7129, Département Adaptations du Vivant, Muséum d'Histoire Naturelle, Centre National de la Recherche Scientifique, Paris, France | [5]Department of Biology, Evolutionary Morphology of Vertebrates, Ghent University, Ghent, Belgium | [6]Naturhistorisches Museum Bern, Bern, Switzerland

Correspondence: Yuri Simone (yurisimone1@gmail.com)

Received: 11 February 2025 | **Revised:** 30 April 2025 | **Accepted:** 4 May 2025

Funding: Y.S. was funded by a PhD scholarship from Fundação para Ciênciae Tecnologia (SFRH/BD/136934/2018). A.v.d.M. was financed through FCT—Fundação para a Ciência e a Tecnologia, I.P. under contract number DL57/2016/CP1440/CT0009.

Keywords: biomechanical model | functional morphology | scorpion chelae | trade-off

ABSTRACT

When selective pressures for different functions act simultaneously on a structure, morphological diversification can be shaped by adaptation toward distinct functional optima. Systems may evolve along a performance gradient, optimizing different aspects of function in response to ecological demands. We investigated two scorpion species representing the morphological extremes of chela (pincer) shape. Scorpion chelae exhibit remarkable morphological diversity associated with ecological roles, and their performance varies along a force-velocity continuum. To explore how structural and muscular adaptations shape performance, we developed a biomechanical model integrating synchrotron microtomography, muscle architecture, and performance data. Our findings reveal that these species exhibit distinct structural and muscular arrangements, each optimized for a different performance outcome. The short-fingered species maximize closing force through increased mechanical advantage and longer sarcomeres, enhancing muscle contraction efficiency. In contrast, the slender-chela species optimizes closing velocity through muscle orientations that favor rapid acceleration. While additional functional demands likely influence these designs, one morphology appears specialized for quickly capturing prey, while the other seems to be adapted for prey crushing. These divergent performance optima may have played a key role in shaping the trophic ecology of scorpions and influencing the evolution of their venom.

1 | Introduction

Morphological diversity is often the result of the necessity to adapt to distinct, and often contrasting, ecological and functional optima (Burress and Muñoz 2023; Holzman et al. 2012; Sansalone et al. 2024; Wainwright 2007). In biomechanical systems, morphological structures frequently evolve toward specialized functional extremes, optimizing performance in one direction while potentially limiting it in another. Systems can diversify by evolving toward alternative performance peaks, where distinct morphologies maximize specific functional outcomes (Garland et al. 2022). Recent evidence suggests that even biomechanical systems, traditionally considered constrained, may exhibit high

evolutionary rates at the extremes of their morphological gradient where typically only a single functional optimum is reached due to the existence of biomechanical trade-offs (Burress and Muñoz 2023; Goswami et al. 2014; Schelp and Burress 2025).

Organismal performance is closely tied to the biomechanical properties of the musculoskeletal system underlying it. Inferring the functional role of specific traits based solely on structural features—such as lever lengths—can lead to oversimplified or potentially misleading conclusions. In static conditions, an increase in mechanical advantage (MA) enhances force output but reduces velocity, shaping a performance gradient between force-optimized and speed-optimized morphologies (Arnold et al. 2011; Herrel et al. 2009; Simone and van der Meijden 2018). However, recent research in muscle dynamics suggests that MA alone is insufficient to fully explain performance, as muscle physiology and architectural constraints can modulate force transmission in a many-to-one fashion, leading to similar outputs despite differences in skeletal mechanics (Labonte 2023; McHenry 2012; Osgood et al. 2021; Polet and Labonte 2024). Numerical simulations have shown that varying one or more architectural variables, such as muscle volume, fiber length, pennation angle, as well as inertial (parasitic) forces, while keeping lever MA constant, can lead to markedly different output velocities (McHenry 2012; Osgood et al. 2021; Polet and Labonte 2024). In addition, a muscle contraction follows a force-velocity gradient, where peak force is generated during isometric contraction, but force declines as contraction velocity increases (Hill 1938).

Arthropods have evolved diverse adaptations to deal with these force-velocity constraints (Osgood et al. 2011a, 2012, 2011b; Osgood et al. 2021). Some taxa, such as pistol shrimps, locusts, and trap-jaw ants, employ elastic energy storage mechanisms to generate rapid, high-power movements (Blanco and Patek 2014; Burrows and Sutton 2012). Alternatively, others decapods exhibit structural asymmetry in their chelae, with one pincer optimized for force and the other for speed, allowing them to balance functional demands across different tasks (Govind et al. 1987; Schenk and Wainwright 2001).

Scorpions provide an exceptional system for studying how functional traits evolve along a morphological gradient, as their body plan compartmentalizes distinct ecological functions into specialized anatomical modules. In contrast to other venomous animals such as snakes, in scorpions, the structures used for subduing prey and venom delivery are on different parts of the body, giving them a higher degree of functional modularity. They grasp prey with their pedipalps (chelae), inject venom using their telson, and process food with their chelicerae. This modular organization allows selective pressures to act more independently on each structure, enabling the pedipalps to evolve toward different performance optima in response to ecological demands such as predation, defense, and intraspecific competition more independently from the other modules (Simone and Meijden 2021). The chelae are formed by the last two segments of the pedipalps, the tibia (or manus) and tarsus (or movable finger). The tibia is the immovable portion and contains most of the muscles responsible for the closing of the chelae. An additional closing muscle is located in the patella, the segment immediately posterior to the tibia (Bicknell et al. 2024; Gilai and Parnas 1970; Snodgrass 1952). Scorpions lack an antagonist set of muscles to open their chelae and the opening is achieved by the elastic recoil of resilin in the joint, and an increase in hydraulic pressure in the manus (Alexander 1967; Govindarajan and Rajulu 1974; Snodgrass 1952). Scorpion chelae exhibit a remarkable morphological diversity, ranging from slender, long-fingered chelae to robust, short-fingered ones (van der Meijden et al. 2010; van der Meijden et al. 2012). While this variation has been linked to habitat use (Coelho et al. 2022), chelae also play key roles in sensing, mating, and intraspecific competition, suggesting that multiple selective pressures contribute to their diversification (Simone and Meijden 2021).

The closing performance of scorpion chelae follows a gradient where long, slender chelae generate high-speed movements but lower force, whereas robust, short-fingered chelae maximize force at the expense of velocity (Simone and van der Meijden 2018). This performance gradient is shaped not only by chela morphology but also by muscle architecture and physiological constraints, which remain largely unexplored (Simone and van der Meijden 2018). In this study, we use volumetric high-resolution scans to examine the architecture of the chela closing muscles in two scorpion species representing the extremes of the morphological gradient. Using these data, we develop a landmark-based biomechanical model to estimate closing force across different degrees of finger rotation. By analyzing muscle and skeletal architecture within and between species, we aim to determine how these traits are finely tuned toward the optimization of specific performance outcomes, namely closing force and velocity.

2 | Materials and Methods

2.1 | Performance Measurements

Scorpio palmatus (Ehrenberg, 1828) and *Hottentotta gentili* (Pallary, 1924) are two scorpion species belonging to the families Scorpionidae and Buthidae, respectively, two phylogenetically distant lineages within the order Scorpiones.

Chela closing forces of *S. palmatus* and *H. gentili* were obtained following van der Meijden et al. (2010) using a Kistler force transducer (Kistler Inc., Winterthur, Switzerland) mounted on a purpose-built holder connected to a charge amplifier as described in Herrel et al. (1999). To measure chela closing velocity, the protocol described in Simone and van der Meijden (2018) was followed. Briefly, the lateral joint and the tips of the fixed and movable fingers were painted with paint enriched with reflective micro glass beads. Subsequently, the scorpion was placed in an arena composed of three orthogonal mirrors and filmed at 500 frames per second from above. Chela closing was stimulated with a thin hair of a small brush. The coordinates of the three landmarks were extracted for the whole

motion using the DLTdv7 package (Hedrick 2008), and kinematic variables were calculated through a customized script in Matlab version R2015a (The MathWorks Inc., Natick, MA, USA). To ensure the achievement of a maximum chela closing performance, five trials per chela were performed for both for closing velocity and force. A recovery time of at least 1 day was maintained between subsequent trials. For this current study, eleven adult individuals of *S. palmatus* and three adult individuals of *H. gentili* were measured to obtain In Vivo chela closing force and velocity. In addition, to compensate for the limited number of *H. gentili* specimens, closing force and morphological data from 10 additional specimens were retrieved from van der Meijden et al. (2010). Closing force, closing duration, angular velocity, and maximum opening angle were used to inform the biomechanical models of finger abduction/adduction built of the two analyzed species representing the extremes of the morphological continuum observed in scorpions (see Data set 1 in Zenodo; https://zenodo.org/records/15312125).

2.2 | 3D Morphological Analysis

2.2.1 | Sample Preparation for Synchrotron Scan

One specimen per species was fixed in 3.7% formaldehyde solution and placed in a small polypropylene tube for X-ray phase contrast synchrotron microtomography (Sr-μCT) as described in Betz et al. (2007). A total of 900 radiographic images were acquired using a FReLoN CCD Camera with an effective pixel resolution of 14.8μm. Beam energy was set at 25 keV and the specimens were scanned at beamline ID19 at the ESRF in Grenoble.

2.2.2 | 3D Volume Rendering and Landmark Definition

All scan data were imported as Tiff-files into Amira (version 5, Mercury Computer Systems Inc., Chelmsford, MA, USA) to generate 3D surfaces of the internal anatomy (ligaments, apodemes, and muscles) and the cuticular elements of both manus and patella.

Per closing muscle, volume was estimated using the module "*Material Statistics*" in Amira. Amira was also used to place specific landmarks (Figure 1A) and to retrieve their 3D coordinates. The landmarks placed at the tip of the movable and fixed finger (MT and FT, respectively) and on the medial and lateral joints (MJ and LJ, respectively) were placed following van der Meijden et al. (2012). Per closing muscle, specific landmarks were placed: the insertion point of the apodeme on the movable finger (apodeme insertion [AI]), the proximal end of the apodeme (AO), the origin and the insertion point on the apodeme of 10 arbitrary fascicles (FO_j and FI_j, respectively) along the whole length of the muscle. The muscle fascicles were modeled as lines passing through each respective FO and FI while the apodemes were modeled as lines passing between AO and AI. In this study, fascicle length was used as a proxy for fiber length since individual segmentation of muscle fibers was not possible due to the scan resolution.

2.3 | Musculoskeletal Model

The musculoskeletal model is based on five main assumptions:

1. All muscles are fully activated simultaneously.
2. Muscle contraction is isovolumetric.
3. Muscles are composed of the same fiber type.
4. The apodeme has a constant length and angle relative to the coordinate system during the whole abduction/adduction event.
5. Muscle stress is constant.

2.3.1 | Data Preparation

The 3D coordinates of the landmarks were imported in Matlab. MJ was chosen as the origin of the reference coordinate system. By subtracting the 3D coordinates of MJ, all the other landmarks were translated to the reference axis having MJ as origin. After this first translation, we placed the LJ on the *x*-axis, to have the rotational axis (the axis passing through MJ and LJ) lying on the *x*-axis. To do so, the coordinates were rotated around the *z*-axis first and subsequently to the *y*-axis using the *rotationmat3d* function (Stanley 2022).

The chelae of the scanned specimens were not constrained to a specific functional opening to avoid damaging the internal organization of the muscles. Consequently, the chelae scanned were naturally fixed at different opening angles; *Scorpio* was almost fully open while *Hottentotta* was almost totally closed. To compare the outputs of the two chela models, the movable fingers of the two scanned species need to be rotated to both be at the natural maximum opening angle. To fully open the chela, the movable finger was rotated around the *x*-axis to the maximum opening angle. Since no performance data were available from the scanned specimens, the maximum opening angle was retrieved from the performance data (see Data set 1 in https://zenodo.org/records/15312125) in specimens that had a similar size (prosoma length) as the scanned ones (Sc3331 for *S. palmatus* and Sc3271 for *H. gentili*).

As a consequence of the last rotation, the apodeme rotated with the movable finger. However, one of the assumptions of the model is that the apodeme has constant length and the angle relative to the coordinate system is kept constant along the whole abduction/adduction event. Therefore, to keep the apodeme at a constant angle, a further rotation of AO around the AI is needed. During closing of the chela, the position of AO must be corrected per degree of rotation. The angle at which rotation takes place is calculated using the following equation:

$$\varepsilon_{(\Psi)} = \operatorname{acos}\frac{\vec{\mu}\cdot\overrightarrow{v_{(\Psi)}}}{\|\vec{\mu}\|\|\vec{v}\|} \quad (1)$$

where the ε_{Ψ} is the angle between the unrotated apodeme and the rotated one per Ψ degrees of rotation and $\vec{\mu}$ and $\vec{v}_j$ are respectively the direction vectors of the unrotated apodeme and

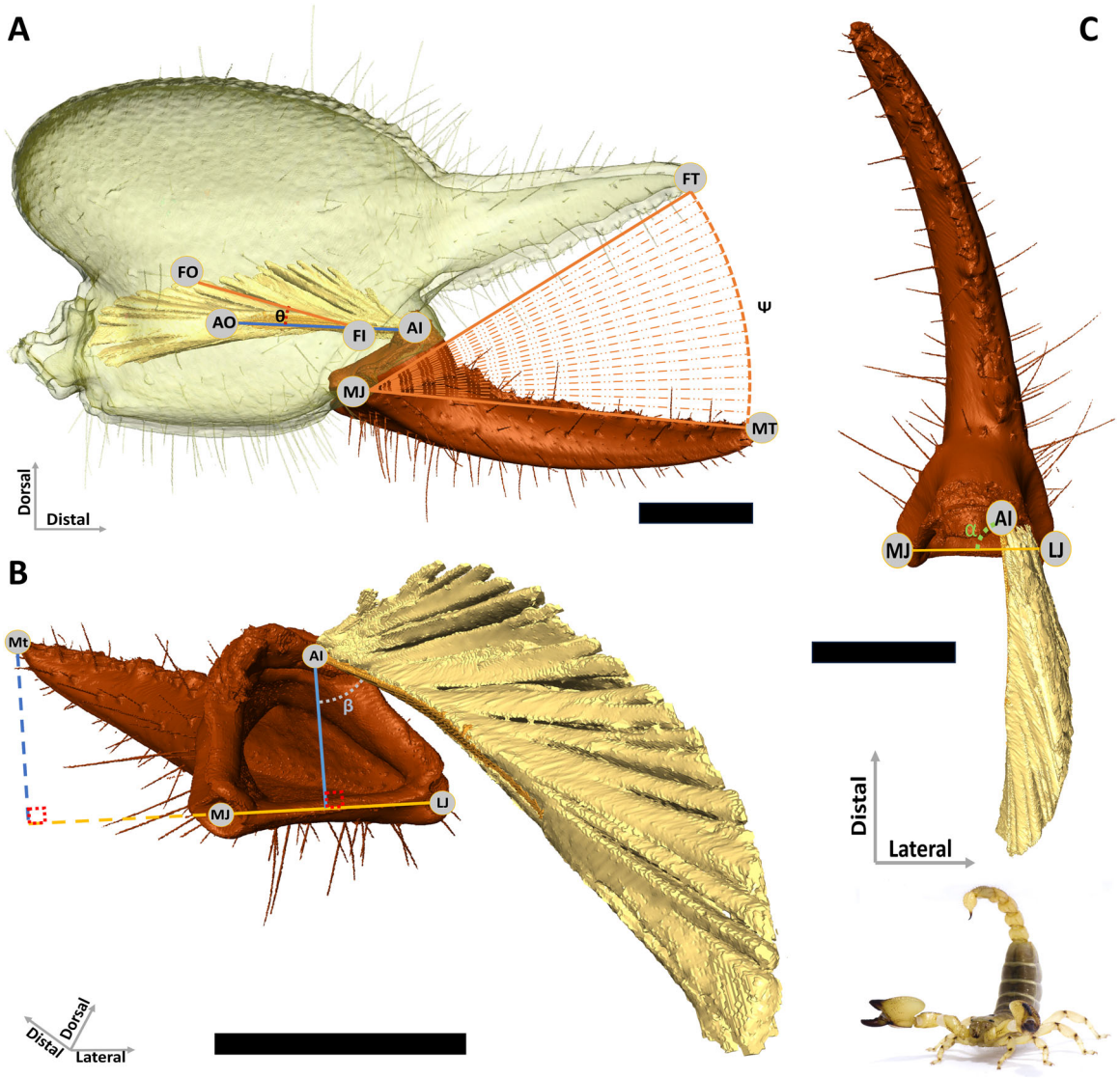

FIGURE 1 | Medial view of the *Scorpio palmatus* chela (A) shows the location of the landmarks used to build the biomechanical model. In (B) and (C), posterior and dorsal view of the movable finger highlight the two insertion angles of the apodeme used to correct bite force estimations. The movable finger is shown in bold brown color, the manus cuticle in transparent gray, the muscle apodeme in orange, and the muscle in yellow. The landmarks applied are: (AI) apodeme insertion; (AO) apodeme origin; (FI) fascicle insertion; (FO) fascicle origin; (FT) fixed finger; (LJ) lateral joint; (MJ) lateral joint; (MT) movable finger; (α) medio-lateral apodeme insertion angle; (β) dorso-ventral apodeme insertion angle; (θ) pennation angle; (Ψ) opening angle. Scale bar = 2 mm.

the rotated one, $\|\vec{\mu}\|$ and $\|\vec{v}\|$ are the magnitude of unrotated and rotated apodeme (which are identical by definition).

Once the angle is calculated, the coordinates of AO and FI_j are rotated around the *x*-axis and the rotated apodeme will be parallel to the unrotated one and FI_j is corrected accordingly.

2.3.2 | Fiber Length and Pennation Angle (Θ)

The fiber length per degree of rotation is calculated as the 3D distance between FO (corresponding to those at the widest opening angle) and FI on the apodeme per degree of rotation.

The pennation angle is defined as the angle between the fiber vector and the apodeme vector.

2.3.3 | MA

MA is the ratio between the effective in-lever and the effective out-lever (calculated per degree of rotation). The effective in-lever was calculated as the minimum perpendicular distance between the long axis of the apodeme and the axis of rotation using the Matlab function *line to line distance* (Douillet 2022). This variable changes its magnitude due to the change of the position of AI and in the dorso-ventral AI angle (β) (see below). The effective in-lever corresponds to the muscle moment arm and was used to calculate the fascicle/moment arm ratio per muscle (Lieber and Ward 2011; Williams et al. 2008). This ratio is largely used in comparative biomechanics to compare how much torque generation varies with rotation extent across muscles with different architectures. Muscles with large fascicle/moment arm ratios generate a nearly constant torque because sarcomere

length changes for a given amount of joint rotation are more limited. However, muscles with small ratios generate large force changes over large joint rotations and more variable torque production (Lieber and Ward 2011; Maganaris et al. 2006).

The effective out-lever was calculated as the minimum distance between the line passing through FT, perpendicular to the axis of rotation using the function *point to line distance* (Rik 2022). Differently from the velocity, which is always calculated at the tip of the movable finger, force is generally measured more proximally. To take this into account, the effective out-lever was shortened by one-third and the MA corrected consequently.

2.3.4 | Physiological Cross-Sectional Area (PCSA)

The calculation of the PCSA is given by the equation:

$$\mathrm{PCSA}_{(\Psi)} = \frac{\mathrm{Volume}}{\mathrm{fiberlength}_{(\Psi)}} \cos\left(\theta_{(\Psi)}\right) \quad (2)$$

This quantity is constant per Ψ degree of rotation. PCSA is a proxy for the number of fibers arranged in parallel within a muscle (Martin et al. 2020). For closing force estimation at each opening angle, we used a fixed value of PCSA retrieved at 15°, which approximately corresponds to the opening angle at which all In Vivo closing force measurements were conducted.

2.3.5 | Dorso-Ventral (β) and Medio-Lateral (α) AI Angle

The dorso-ventral β is the angle defined by the apodeme vector and the in-lever vector (Figure 1B). The apodeme's orientation relative to the in-lever might be a source of force loss due to the two force components that do not contribute to the rotation. These components of the force are loaded onto the joints and are not available for rotation. The only component of the muscle input force that is transmitted to the out-lever is the sin(β). The medio-lateral orientation of the apodeme vector and the axis of rotation (α) is another source of force loss (Figure 1C). Differently from β, this angle remains constant. Only the sin(α) is transmitted to the out-lever.

2.3.6 | Muscle Stress (Σ)

Muscle stress (σ) is the force per unit of cross-sectional area that a muscle can exert. It depends on the contractile state of the sarcomeres (Rospars and Meyer-Vernet 2016), but in this model, it will be kept constant along sarcomere contraction.

To estimate muscle stress, two different approaches were followed. The first approach consists of estimating muscle stress as the ratio between the total closing force at the insertion on the movable finger and the sum of all PCSAs. Since closing force is unknown for the scanned specimens, it was estimated using the method described in Bicknell et al. (2022). All the closing forces of the scanned specimens were inferred at an opening angle of 15°.

For the second approach to estimate muscle stress, we performed a reduced major axis regression (RMA) using the log-transformed sarcomere length as the independent variable and the log-transformed muscle stress as the response variable. A regression equation in the form $Y = a + bX$ was created using the muscle stresses and the sarcomere lengths from (Taylor 2000), with a and b the RMA intercept and slope, respectively. To obtain the stress of the scanned species, X was substituted with the log-transformed mean sarcomere length measured of each scanned species (sarcomere length measurements are detailed further below). To transform the value of the stress from log-scale to the original scale (kPa), we calculated 10^{Y}. This analysis was inspired by Püffel et al. (2023).

2.3.7 | Closing Force Estimation

Once the muscle stress is calculated, it is possible to estimate the closing force at the out-lever generated by each muscle per degree of rotation taking into account the effect of the geometric orientation of each muscle, resulting in the following equation:

$$F_{(\Psi)} = \mathrm{PCSA} \times \mathrm{MA}_{(\Psi)} \times \sin(\alpha) \times \sin(\beta)_{(\Psi)}\, x\, \sigma \quad (3)$$

To compare the two approaches, the closing force was calculated using the two different estimated values of muscle stress.

2.4 | Sarcomere Length Measurements

To measure sarcomere length in the two analyzed species, the manus and patellar closing muscles of four adult specimens for each species (eight chelae per species) were dissected on a Leica M80 stereomicroscope. All specimens were euthanized by exposure to isoflurane vapors to ensure complete relaxation of the pedipalp muscles. Manus closing muscles were divided into four different groups: dorsal, lateral, medial, and ventral aiming to isolate muscle with long, intermediate, and short moment arms. Each group of dissected muscles was placed in a 30% aqueous solution of HNO_3 at 10°C to dissolve the connective tissue surrounding the muscle fascicles. After 48 h the nitric acid was removed and substituted with 50% aqueous solution of glycerol, and individual fibers were separated with a dissection probe and moved to a microscope slide.

Microscopic pictures of individual fibers were taken using an Axio zoom V16 microscope (Carl Zeiss Microscopy GmbH, Göttingen, Germany) mounted with an Axio cam MRc5 at the Centre de Microscopie de fluorescence et d' IMagerie numérique (CeMIM, Paris). Images of individual fibers were magnified up to 270 times, magnification at which the A band of sarcomeres was distinctly visible (Figure S1A). To reduce mistakes in focusing, a stack of 100 planes (total stack height = 100 μm) was compiled through the ZEN pro software (blue edition). Stacks were loaded in Fiji (Schindelin et al. 2012), and a straight line perpendicular to the A bands was drawn to obtain a pixel intensity plot along the length of the drawn line. The pixel intensity plot has the

value in gray scale of the pixel on the vertical axis and the position in micrometers along the line on the horizontal axis. This set of 2D coordinates was extracted and loaded into a custom script in R. The script applies a low-pass fourth-order Butterworth filter with a cutoff frequency of 15 Hz. By using the function *findpeaks* from the package "gsignal" (Van Boxtel et al. 2021), the coordinates of the top peaks were retrieved and the distance on the *x*-axis between two consecutive peaks was calculated as individual sarcomere length (an example is provided in Figure S1B,C).

2.5 | Statistical Analysis

All statistical analysis were performed in R version 4.2.2 (R Development Core Team 2022).

2.6 | Within-Species Analysis

We performed Student *t*-tests to assess whether significant differences in sarcomere length exist across manus and patellar closing muscles within species. Moreover, we also performed linear models (ANOVA) within and across the two scanned species to test for differences in sarcomere length across the four different muscle groups (dorsal, lateral, medial, and ventral).

2.7 | Analysis Across the Scanned Species

We used Student *t*-tests to test for differences in sarcomere length, pennation angles, MA, and fascicle moment arm ratio between the two scanned species. Since not all the variables had a normal distribution of residuals and lacked homoscedasticity, all the variables were normalized through $\log_{10}$ transformation before running the Student *t*-test. Moreover, we were also interested in detecting patterns of pairwise covariation of the four most representative muscle architecture variables: fiber length, pennation angle, PCSA, and moment arm. To quantify and visualize patterns of covariation, a pairwise correlation matrix of these variables was built. The correlation coefficients were calculated and graphically compared among the two species analyzed. The pairwise correlation coefficients and their significance were retrieved through the function *ggpairs* of the package "GGally" (Schloerke et al. 2021) considering a corrected alpha of 0.008 following Bonferroni's correction for repeated tests. The same package was also used to plot the correlation matrix.

3 | Results

3.1 | Performance Data

Angular velocity was on average 26.6 ± 5.48 rad/s (mean $\pm$ sd) in *S. palmatus* and 38.5 ± 10.5 rad/s in *H. gentili* while closing force was on average 8.00 ± 1.76 N in *S. palmatus* and 0.58 ± 0.06 N in *H. gentili*.

3.2 | Muscle Architecture in the Scanned Species

The muscle architecture across the two scanned species shows remarkable differences (Figure 2). One of the more striking differences is the relative size of the patellar muscle in the two species, representing 49% of the volume of all closing muscles in *Hottentotta* but only 1.5% in *Scorpio* (see Table 1).

The number of muscles within the manus differs between the two scanned species. In *Scorpio*, a total of 14 distinct muscles were identified whereas only 12 in *Hottentotta*. The pairwise correlation matrix of the four analyzed muscle architecture variables showed an overall absence of significant patterns among them. However, the most remarkable finding is the distinct correlation pattern between moment arm and PCSA in the two species. In *Hottentotta*, this pattern is negative and highly significant ($\alpha = -0.857$) meaning that in this species the strongest muscles typically have shorter moment arms. Conversely, in *Scorpio* moment arm and PCSA are positively correlated ($\alpha = 0.651$) indicating that strongest muscles in this species are inserted with longer moment arms (see Figure 3).

Average pennation angles in manus closing muscles in *Hottentotta* show a tendency of being smaller than those in *Scorpio* (*Hottentotta* $18.6° \pm 5.15°$; *Scorpio* $23.7° \pm 8.14°$; $p = 0.062$). There is no statistical difference between the two species in the fascicle length/moment arm ratio ($p = 0.45$). However, Figure S2 shows that, within manus closing muscles, this index is less heterogeneous in *Hottentotta* compared to *Scorpio*. In the latter species, three muscles present particularly larger fascicle length/moment arm ratios compared to the rest (see Table 1).

Sarcomeres are significantly longer in *Scorpio* than in *Hottentotta* ($p < 0.001$). In both species the sarcomeres of the manus closing muscles are longer than those measured in the patellar muscle (see Figure 4A). Moreover, sarcomere length is not evenly distributed across the four distinct groups of manus closing muscles (see Figure 4B). In *Hottentotta*, sarcomeres from muscles with a longer moment arm (dorsal) are shorter than sarcomeres measured from muscles with shorter moment arm (ventral). The opposite is observed in *Scorpio*. The results of the statistical tests are summarized in Tables S1–3.

3.3 | Model Output

The muscle stress estimated from the biomechanical model is 841 KPa in *Scorpio* and 897 KPa in *Hottentotta*. The muscle stress estimated from the RMA model is 339 KPa in *Scorpio* while it is 257 KPa in *Hottentotta*.

Despite the sarcomere force-length relationship not having been taken into account, from pure geometrical considerations on muscle orientation about the rotational axis, it seems that the opening angle has an important effect on closing force. The estimated closing force per degree of closing angle shows indeed remarkable differences between the two species. The peak value of closing force is reached at larger opening angles in

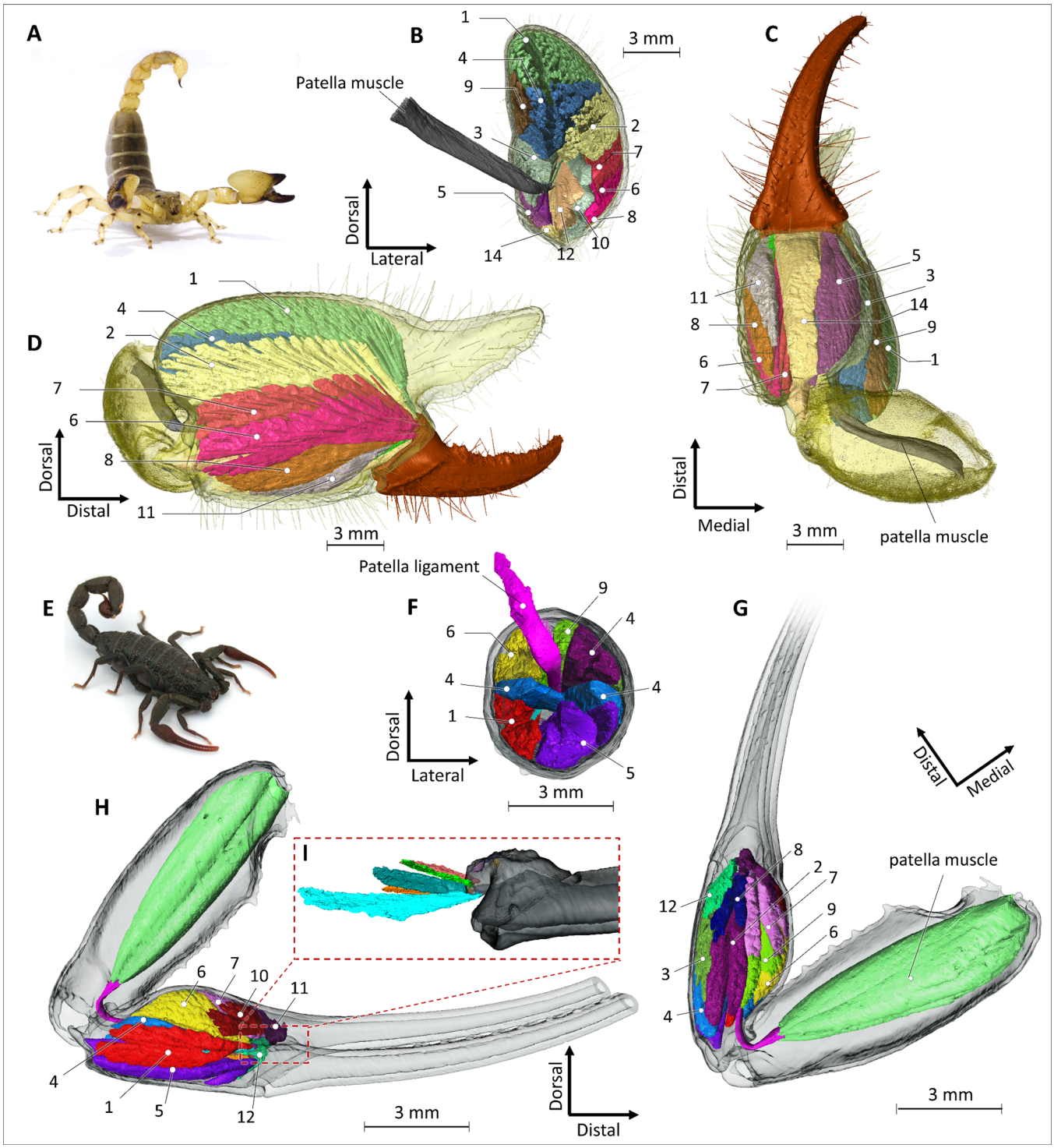

FIGURE 2 | Comparison of chela closing muscle architecture in two scorpion species. Live habitus of *Scorpio palmatus* (A) and *Hottentotta gentili* (E). Solid 3D volumes represent the chela closing muscles, with each muscle reconstructed in its natural configuration. The cuticle has been rendered transparent to facilitate visualization of the underlying musculature. Posterior (B), ventral (C), and lateral (D) views of the chela closing muscles in *S. palmatus*. Posterior (F), ventral (G), and lateral (H) views of the chela closing muscles in *H. gentili*. (I) Close-up of the proximal portion of the movable finger in *H. gentili*, showing the sclerotized bulge that enables muscle insertion at very small moment arms. Numbers correspond to muscle identities as listed in Table 1.

Hottentotta (44°) while in *Scorpio* peak closing force is reached at medium opening angles (18°). The profile in Figure 5 also shows how, following the peak force, a substantial decline in force takes place in *Hottentotta*. In *Scorpio*, the decrease in force after the peak is not as pronounced.

Muscles in *Scorpio* are inserted with a greater MA than the muscles in *Hottentotta*. Moreover, the maximum MA is generally reached at the beginning of the closing event in *Hottentotta* while in *Scorpio* peak MA is reached when the chela is almost fully closed.

TABLE 1 | Summary table of kinematic and physiological variables measured for the two scanned species.

Species	Muscle	Fiber length (m)	PA (°)	MA	Moment arm (m)	β (°)	α (°)	ACSA (m^2)	PCSA (m^2)	Volume (m^3)	% Vol total	Fascicle/ moment arm
Hottentotta gentili	1	1.56E−03	22.9	0.078	7.20E−04	97.0	96.5	8.67E−07	7.98E−07	1.35E−09	5.40	1.94
	2	2.03E−03	12.8	0.095	8.70E−04	114	92.7	8.20E−07	8.05E−07	1.70E−09	6.78	2.34
	3	1.94E−03	11.8	0.092	8.48E−04	103	79.9	5.13E−07	5.02E−07	8.72E−10	3.48	2.29
	4	2.18E−03	26.6	0.087	8.00E−04	108	88.2	7.19E−07	6.42E−07	1.58E−09	6.29	2.72
	5	1.89E−03	24.3	0.078	7.21E−04	93.8	91.1	1.35E−06	1.23E−06	2.55E−09	10.2	2.62
	6	1.86E−03	18.8	0.093	8.51E−04	107	108	7.43E−07	7.03E−07	1.40E-09	5.56	2.19
	7	1.43E−03	19.2	0.091	8.33E−04	125	105	6.70E−07	6.33E−07	9.96E−10	3.97	1.71
	8	1.58E−03	11.6	0.105	9.68E−04	112	86.7	3.55E−07	3.48E−07	5.75E−10	2.29	1.63
	9	1.99E−03	13.9	0.090	8.29E−04	120	106	4.68E−07	4.55E−07	9.56E−10	3.81	2.40
	10	1.71E−03	22.2	0.105	9.65E−04	75.8	122	1.48E−07	1.37E−07	2.52E−10	1.01	1.77
	11	1.60E−03	17.6	0.114	1.05E−03	85.5	74.7	2.07E−07	1.97E−07	3.31E−10	1.32	1.53
	12	1.79E−03	22.0	0.146	1.34E−03	110	83.4	1.56E−07	1.45E−07	2.20E−10	0.878	1.34
	pat	7.62E−03	0.0	0.110	1.01E−03	104	96.6	1.54E−06	1.46E−06	1.23E−08	49.0	7.53
Scorpio palmatus	1	2.60E−03	31.3	0.361	2.07E−03	98.9	98.3	7.17E−06	6.13E−06	1.84E−08	29.4	1.25
	2	3.05E−03	34.2	0.341	1.95E−03	85.0	89.9	2.13E−06	1.76E−06	6.45E−09	10.3	1.56
	3	2.34E−03	20.5	0.247	1.41E−03	80.2	91.6	1.74E−06	1.63E−06	4.01E−09	6.41	1.66
	4	2.95E−03	21.5	0.306	1.75E−03	108	88.2	2.04E−06	1.90E−06	5.96E−09	9.52	1.68
	5	2.08E-03	25.3	0.216	1.24E−03	69.2	81.8	1.23E−06	1.11E−06	2.53E−09	4.04	1.68
	6	1.96E−03	26.8	0.283	1.62E−03	75.0	79.5	1.81E−06	1.61E−06	3.50E−09	5.59	1.21
	7	2.17E−03	25.7	0.321	1.84E−03	83.7	79.1	1.24E−06	1.12E−06	2.65E−09	4.23	1.18
	8	1.56E−03	30.6	0.250	1.43E−03	67.9	77.2	1.10E−06	9.51E−07	1.71E−09	2.73	1.09
	9	2.22E−03	24.9	0.294	1.68E−03	98.3	97.3	1.48E−06	1.34E−06	3.24E−09	5.18	1.32
	10	3.57E−03	15.5	0.242	1.39E−03	62.0	85.8	9.96E−07	9.63E−07	4.08E−09	6.51	2.58
	11	1.20E−03	35.0	0.221	1.27E−03	57.8	76.9	7.17E−07	5.87E−07	5.23E−09	8.36	0.95
	12	2.37E−03	18.7	0.288	1.65E−03	117	114	4.51E−07	4.27E−07	8.54E−10	1.36	1.44
	13	5.45E−03	5.29	0.224	1.28E−03	67.6	79.2	3.74E−07	3.71E−07	1.06E−09	1.69	4.25
	14	4.91E−03	16.3	0.240	1.37E−03	62.0	85.8	1.07E−06	1.03E−06	2.03E−09	3.24	3.58
	pat	4.50E−03	0.0	0.295	1.69E−03	80.6	88.6	1.98E−07	1.98E−07	8.86E−10	1.41	2.66

Abbreviations: %Vol, percentage of muscle volume on the total volume of closing muscles; α, medio-lateral apodeme insertion angle; β, dorso-ventral apodeme insertion angle; ACSA, anatomical cross-sectional area; MA, mechanical advantage; PA, pennation angle; pat, patella muscle; PCSA, physiological cross-sectional area.

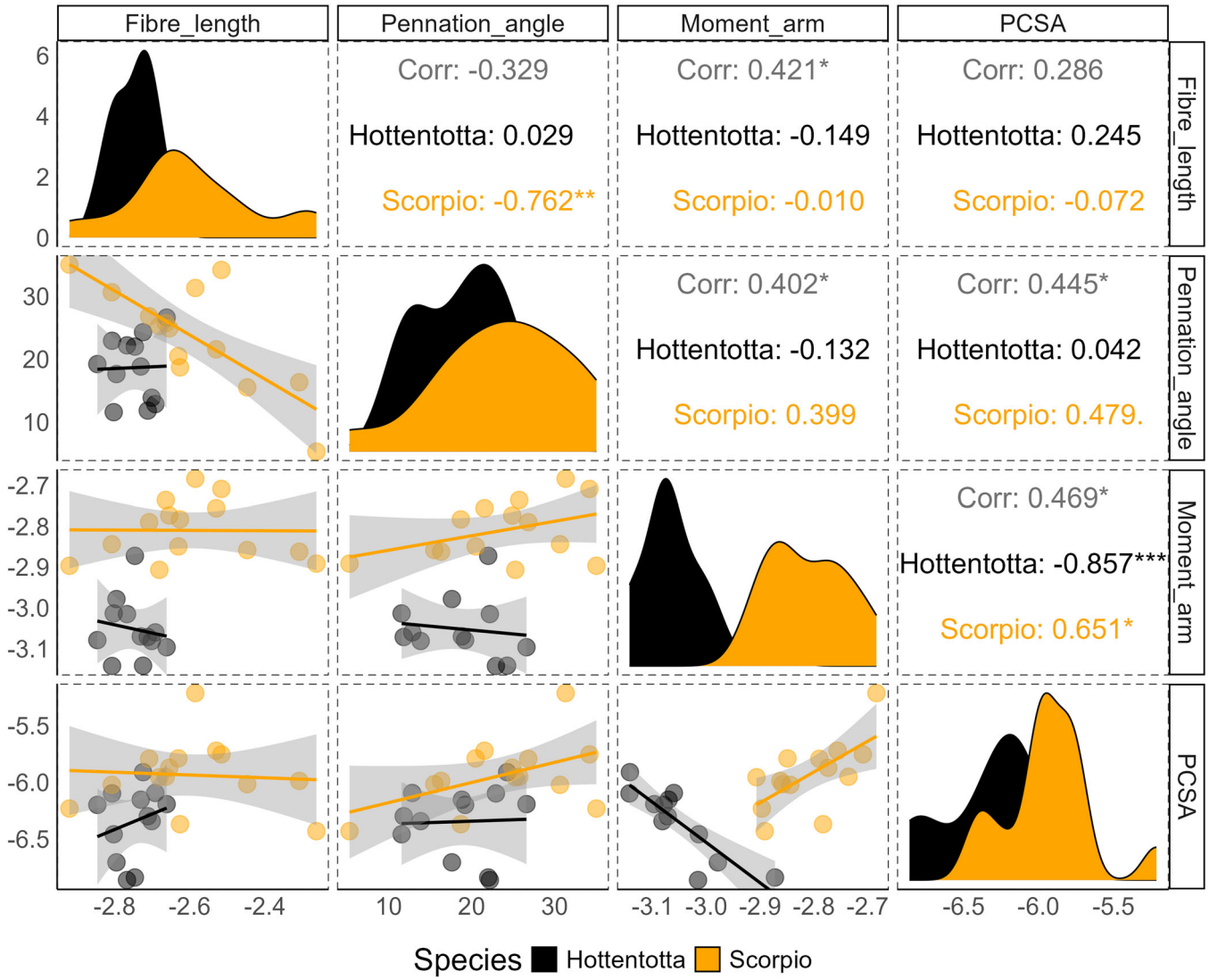

FIGURE 3 | Pairwise correlation plot across four determinants of architectural muscle: fiber length, pennation angle, moment arm, and PCSA. Asterisks show the level of significance relative to a corrected α of 0.008 after Bonferroni's correction.

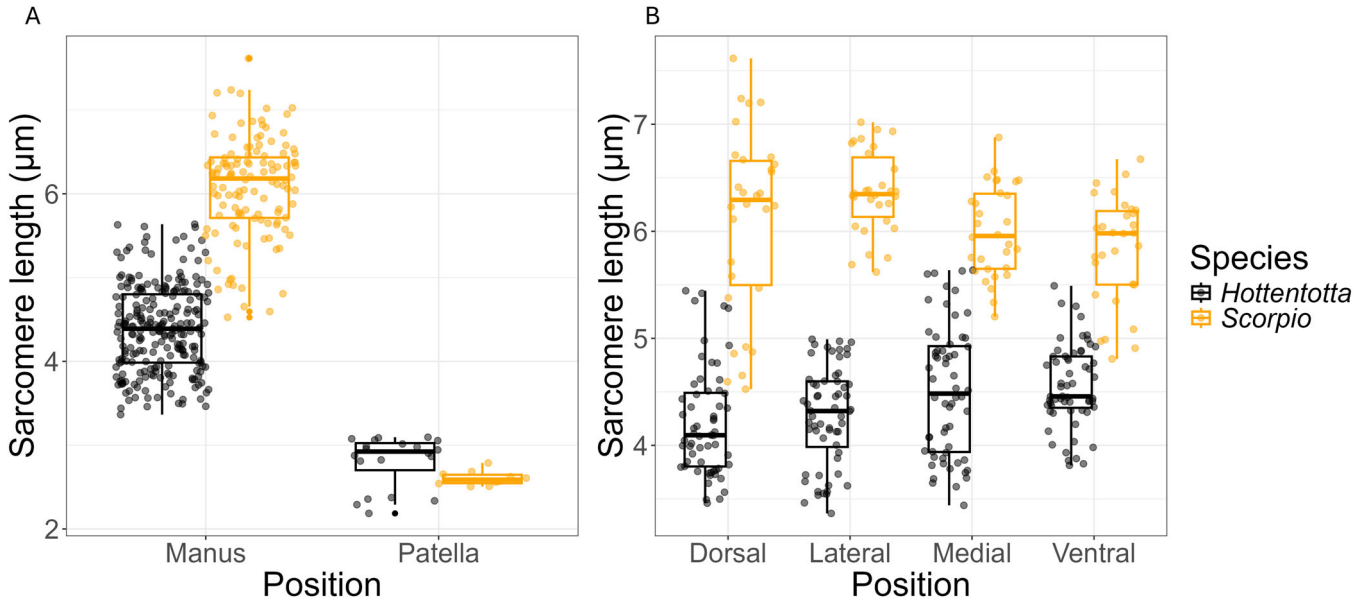

FIGURE 4 | (A) Manus and patella sarcomere length across *Hottentotta* (black boxplots and dots) and *Scorpio* (orange boxplots and dots). (B) Sarcomere length across species grouped by different locations in the manus.

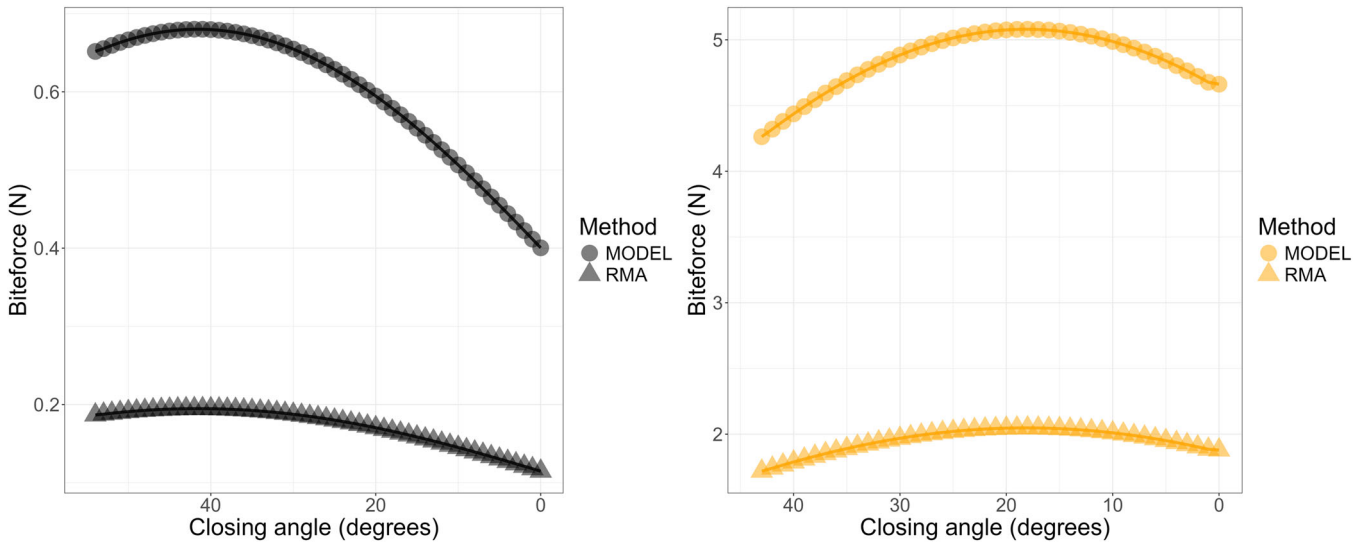

FIGURE 5 | Force generated per closing degree in *Hottentotta* (black) and *Scorpio* (orange). The different marker shapes represent the estimation of the force with stress calculated using the RMA method (triangles) and from the model (circles).

4 | Discussion

In this study, the biomechanical determinants of chela closing performance were analyzed in two species of scorpion with contrasting chela morphologies. We generated 3D models of the chelae of both scanned species and found contrasting patterns in the arrangement, architecture, and MA of the closing muscles and the structural elements. Each species seems to converge on the optimization of a different aspect of chela closing performance: closing force in the robust-chela species *S. palmatus* and closing velocity in the slender-chela species *H. gentili*. This is evident from each separate variable we considered in this study: MA, muscle architecture and gearing, and sarcomere length. These variables, at least among the two species selected as representative of chela morphological gradient, are geared in a coordinated manner to maximize either the force or the velocity functional optima.

4.1 | Closing Muscles in Slender-Chela Species Are Geared for Rapid Acceleration

The most important difference observed is the inverse relationship between PCSA and muscle moment arm. In *Hottentotta,* the strongest muscles are those with shorter moment arms. These muscles are attached to the ventral part of a sclerotized bulge located in the proximal portion of the movable finger which is absent in *Scorpio* (see Figure 2). During fast rotations, muscles with shorter moment arms may still generate large torques about a joint due to their reduced shortening rates (Nagano and Komura 2003). Due to the force-velocity relationship, the muscles with lower shortening rates generate relatively more tension than the muscles with higher shortening rates (Lieber and Ward 2011). Muscles with short moment arms have reduced sarcomere shortening, making them operate primarily on the plateau and the beginning of the descending limb of their length-tension curve (Lieber and Ward 2011; Lieber et al. 1997). Therefore, it seems that the larger PCSA and the longer sarcomeres, compared to the mean sarcomere length, can be hypothesized as compensatory solutions to the loss of torque due to the short moment arms. The slow contraction coupled with larger PCSAs, relatively longer sarcomeres in muscles with shorter moment arms, great fascicle-to-moment arm ratios, and the highest MA reached at large opening angles, make these muscles better designed to generate large angular acceleration in the first phases of the chela closing.

4.2 | Functional Specialization: *H. gentili* Versus High-Performance Sprinters

The architecture of the chela closing muscles in *H. gentili* shares features in common with the muscle architecture of specialized sprinters. The lateral gastrocnemius of professional runners (Lee and Piazza 2009; Nagano and Komura 2003), the muscles of the thoracic limbs in greyhound dogs (Williams et al. 2008) and the ankle muscles in ostrich (Smith et al. 2006) are similarly designed to the chela closing muscles of *H. gentili*, typically with high fascicle-to-moment arm ratios and generating great power peaks to promote explosive acceleration. Differently from *Hottentotta*, the specialized sprinters need to generate a large joint torque to counterbalance the ground reaction force and the inertia due to the limb mass (Alexander 2006). In *Hottentotta*, as in *Scorpio*, the force generated by the muscles is much larger than the "parasitic forces" (e.g., the moment of inertia of the movable finger and the resistance exerted by the air; Labonte 2023; Polet and Labonte 2024). Therefore, the force generated at the beginning of the rotation is almost entirely used to accelerate the movable finger. In high-load contractions, this muscle design is not as effective. In this condition, muscles generally contract almost isometrically. Therefore, to generate greater tension, muscles with larger PCSAs and inserted with longer moment arms are necessary. However, in *H. gentili*, the muscles with longer moment arms are those having the smallest PCSA and relatively shorter sarcomeres.

4.3 | The Patellar Closing Muscle: A Versatile Contributor Across Load Conditions

An important contribution to chela closing performance is provided by the patellar closing muscle. This muscle might play a crucial role in both low- and high-load contraction. The patellar closing muscle

is a parallel-fibered muscle with short sarcomeres which allows fast contraction. In the patella, it also has more space to grow longer, allowing for a faster contraction. In *Hottentotta*, this muscle comprises 49% of the volume of all closing muscles and is inserted on the movable finger with a relatively long moment arm. The greater length and short sarcomeres of this muscle suggest it contracts fast, and it may therefore be less hampered to contribute to rapid closing by a high MA than the shorter muscles of the chela manus would be. Its relatively large cross-sectional area, combined with an advantageous MA, would still allow a fair (static) force to be generated by this muscle, for example, for holding prey.

4.4 | Closing Muscles in Robust-Chela Species Are Geared for Large Crushing Force

The chela closing muscles in *S. palmatus* appear remarkably suitable for generating high forces under nearly isometric conditions (e.g., when the chela is partially or nearly fully closed and holding a prey). This is primarily due to the positive correlation between PCSA and muscle moment arm. These muscles not only possess the theoretical capability to generate high force, but they are also inserted with longer moment arms, consequently resulting in a large force at the chela movable finger (Lieber and Ward 2011; Powell et al. 1984). Furthermore, these muscles have also long sarcomeres. Longer sarcomeres generate more actin-myosin cross bridges and consequently can generate a higher tension (Huxley 1957). However, under low-load conditions, muscles with longer moment arms must contract faster than those having a shorter moment arm, thereby developing smaller forces and consequently torques about the joint (Nagano and Komura 2003; Osgood et al. 2021).

4.5 | Muscle Architecture and Gearing Flexibility in *S. palmatus*

In *S. palmatus*, the fascicle-to-moment arm ratio of the chela closing muscles reveals an interesting pattern absent in *H. gentili*. While all muscles in *Scorpio* have small fascicle to moment arm ratios, three of the muscles (10, 13, and 14) having the shortest moment arm also have the largest fascicle/moment arm ratio values (Figure S2**)**. They present a typical design of fast contracting muscles in being long, almost parallel fibered, and with relatively shorter sarcomeres (Gans 1982). It seems thus that in *Scorpio*, but not in *Hottentotta*, two distinct categories of muscles exist: the first is designed to optimize force generation and is dorsally located in the chela, while the second group, ventrally located, is more suited to produce fast contraction. Synergistic muscles with different architectures provide some sort of gearing flexibility according to the different mechanical needs (Lieber et al. 1997; Wakeling et al. 2011). However, in *Scorpio* the muscles designed to produce higher closing forces take up about 88% of the volume of all closing muscles. This disparity between the two muscle categories thus indicates that strong rather than faster chela closing is the predominant functional need in *Scorpio*. This is further underscored by the relative volume of the patellar muscle, which accounts for only 1.41% of the total closing muscle volume, making it the second smallest closing muscle. Although its structural features, parallel fibers and shorter sarcomeres compared to *Hottentotta*—suggest a role in fast closure, its minimal size renders this contribution functionally negligible. These findings highlight how the specialization for powerful closure in *Scorpio* has led to the near vestigiality of the patellar muscle.

4.6 | Correlation Between Sarcomere Length and Chela Closing Force

The sarcomere length in the manus of the two scanned species suggests a positive correlation between sarcomere length and chela closing force (Alexander 2006). This pattern has been observed in many groups of crustaceans. Specifically, in the chelae of crabs (Taylor 2000), in the raptorial appendages of mantis shrimps (Blanco and Patek 2014) and, within the same individual, across the crusher and the cutter chelae of adult lobsters (Govind and Lang 1978). The sarcomere length variation between the two species ranges from 3 to 6 μm indicating that from the shortest to the longest sarcomere length there is a doubling (100%) of force generation. This variation is only 50% across the spearers and smashers mantis shrimps (Blanco and Patek 2014) and only 60% across the crabs. This result supports the idea that chela closing muscles in fast and strong species evolved toward an optimization or either velocity or force. Contrary to manus muscles, there is a striking uniformity in the sarcomere length of the patellar muscle across species. This suggests that this muscle evolved in all scorpions to facilitate rapid finger abduction. However, in species with rapid closure, the necessity for force has led to the increasing of the PCSA of the closing patellar muscle while in species with strong chela closing, since velocity is not a priority, this muscle is relatively small.

4.7 | Biomechanical Consequences for Feeding Ecology

The distinct chela designs and markedly diverse closing muscle architectures observed in the two scanned species suggest that chelae are optimized for distinct predatory strategy and to capture different prey types as already observed in other grasping appendages in arthropods (Blanco and Patek 2014; Bowman 2021; Freire et al. 1996; Schenk and Wainwright 2001; Behrens Yamada and Boulding 1998). Specifically, the force distribution across the entire closing event in *Hottentotta* shows a force peak during the initial phases, followed by a significant decline during the central phase of the event. This suggests that in this species, muscle architecture of closing muscles and the elongated chela fingers are designed for a quick grasping of the prey rather than for a strong holding or crushing (Simone and van der Meijden 2018; van der Meijden et al. 2010). In contrast, in the robust-chela species the peak force is generated in the middle of the closing event, when prey has been already seized, and the decrease in force toward the final phases is minimal. Consequently, the slender-chela species relies not on force for holding prey, but rather on the efficacy of its venom (Evans et al. 2019; García et al. 2022). The potent and rapid-acting venom plays a pivotal role in immobilizing the prey and diminishing the chances of escape. In addition to venom, friction can have an important role in prey holding. The numerous

rows of small denticles on the fingers of *Hottentotta* and other slender-fingered buthids are likely to enhance the friction, thereby increasing the grip on the prey's body (Wolff and Gorb 2016). Conversely, the robust chelae species such as *Scorpio* have large interlocking saw-teeth on the finger, increasing local pressure and the shear forces on the body of the prey (Bowman 2021). Another line of evidence that points to crushing rather than just holding is that prey subduing often happens without venom expenditure in the robust-chela species (Casper 1985; Schultze 1927).

We acknowledge that a two-species comparison alone is not sufficient to infer broad-scale adaptation across an entire clade (Garland and Adolph 1994). However, our results, based on high-resolution imaging, biomechanical modeling, and performance data, strongly suggest that the observed functional divergence may reflect an adaptive response to distinct ecological pressures. Moreover, our findings reveal a possible fundamental trade-off between rapid grasping and holding versus crushing mechanisms, which may have profoundly influenced scorpion predatory behavior and venom evolution. Different predatory performances might also correspond to different prey preferences, but diet in scorpions remains a challenging and largely unexplored field due to technical limitations. Advances in molecular techniques for retrieving prey DNA from scorpion digestive tracts (Simone et al. 2022) may soon allow researchers to test whether species with contrasting chela morphology also occupy distinct foraging niches.

5 | Conclusions

Our findings clearly show how divergent functional demands can drive the evolution of specialized biomechanical systems within a single clade. The evidence presented here supports the hypothesis that scorpion chelae are subject to selective pressures that optimize them for either forceful crushing or rapid, high-acceleration closures, leading to two distinct performance optima within the group. In species with robust chelae, like *S. palmatus*, muscle architecture is geared toward generating high force, including larger cross-sectional muscle areas, longer moment arms, and longer sarcomeres, all of which contribute to greater bite force. Conversely, in species with slender chelae, like *H. gentili*, muscle architecture is optimized for velocity through larger PCSA, shorter moment arms, and overall shorter sarcomeres.

Author Contributions

Yuri Simone: conceptualization, data curation, writing – original draft, formal analysis, methodology, writing – review and editing, investigation, software, validation, visualization. **Anthony Herrel:** conceptualization, funding acquisition, resources, supervision, validation, writing – review and editing. **Renaud Boistel:** methodology, resources. **Arie van der Meijden:** conceptualization, funding acquisition, investigation, methodology, project administration, resources, supervision, validation, writing – review and editing.

Acknowledgments

We are grateful to Cyril Willig and Marc Gèze for the use of the microscope of the CeMIM, Paris. Y.S. was funded by a PhD scholarship from Fundação para Ciênciae Tecnologia (SFRH/BD/136934/2018). A.v.d.M. was financed through FCT—Fundação para a Ciência e a Tecnologia, I.P. under contract number DL57/2016/CP1440/CT0009.

Ethics Statement

The authors have nothing to report.

Conflicts of Interest

The authors declare no conflicts of interest.

Peer Review

The peer review history for this article is available at https://www.webofscience.com/api/gateway/wos/peer-review/10.1002/jmor.70055.

Data Availability Statement

All relevant data and resources can be found within the article and its supporting information. Data sets and scripts can be found in Zenodo https://zenodo.org/records/15312125.

References

Alexander, A. J. 1967. "Problems of Limb Extension in the Scorpion, Opisthophthalmus *Latimanus koch*." *Transactions of the Royal Society of South Africa* 37: 165–181.

Alexander, R. M. 2006. *Principles of Animal Locomotion*. Princeton University Press.

Arnold, A. S., C. T. Richards, I. G. Ros, and A. A. Biewener. 2011. "There Is Always a Trade-Off Between Speed and Force in a Lever System: Comment on McHenry (2010)." *Biology Letters* 7: 878–879.

Behrens Yamada, S., and E. G. Boulding. 1998. "Claw Morphology, Prey Size Selection and Foraging Efficiency in Generalist and Specialist Shell-Breaking Crabs." *Journal of Experimental Marine Biology and Ecology* 220: 191–211.

Betz, O., U. Wegst, D. Weide, et al. 2007. "Imaging Applications of Synchrotron X-Ray Phase-Contrast Microtomography in Biological Morphology and Biomaterials Science." *Journal of Microscopy* 227: 51–71.

Bicknell, R. D. C., G. D. Edgecombe, C. H. R. Goatley, G. Charlton, and J. R. Paterson. 2024. "Pedipalp Anatomy of the Australian Black Rock Scorpion, *Urodacus manicatus*, With Implications for Functional Morphology." *Australian Journal of Zoology* 72: ZO23044. https://doi.org/10.1071/ZO23044.

Bicknell, R. D. C., Y. Simone, A. van der Meijden, S. Wroe, G. D. Edgecombe, and J. R. Paterson. 2022. "Biomechanical Analyses of Pterygotid Sea Scorpion Chelicerae Uncover Predatory Specialisation Within Eurypterids." *PeerJ* 10: e14515.

Blanco, M. M., and S. N. Patek. 2014. "Muscle Trade-Offs in a Power-Amplified Prey Capture System." *Evolution* 68: 1399–1414.

Bowman, C. E. 2021. "Feeding Design in Free-Living Mesostigmatid Chelicerae (Acari: Anactinotrichida)." *Experimental and Applied Acarology* 84: 1–119.

Van Boxtel, G., R. Laboissière, and H. D. Wilhelm. 2021. Gsignal: Signal Processing [Computer Software]. https://github.com/gjmvanboxtel/gsignal.

Burress, E. D., and M. M. Muñoz. 2023. "Functional Trade-Offs Asymmetrically Promote Phenotypic Evolution." *Systematic Biology* 72: 150–160.

Burrows, M., and G. P. Sutton. 2012. "Locusts Use a Composite of Resilin and Hard Cuticle as an Energy Store for Jumping and Kicking." *Journal of Experimental Biology* 215: 3501–3512.

Casper, G. 1985. "Prey Capture and Stinging Behavior in the Emperor Scorpion, *Pandinus imperator* (Koch) (Scorpiones, Scorpionidae)." *Journal of Arachnology* 13: 277–283.

Coelho, P., A. Kaliontzopoulou, P. Sousa, M. Stockmann, and A. van der Meijden. 2022. "Reevaluating Scorpion Ecomorphs Using a Naïve Approach." *BMC Ecology and Evolution* 22: 17.

Douillet, N. 2022. Line to Line Distance (3D) [Computer Software]. https://github.com/NicolasDouillet/line_to_line_distance/releases/tag/v1.3.

Evans, E. R. J., T. D. Northfield, N. L. Daly, and D. T. Wilson. 2019. "Venom Costs and Optimization in Scorpions." *Frontiers in Ecology and Evolution* 7: 1–7.

Freire, J., M. Sampedro, and E. González-Gurriarán. 1996. "Influence of Morphometry and Biomechanics on Diet Selection in Three Portunid Crabs." *Marine Ecology Progress Series* 137: 111–121.

Gans, C. 1982. "Fiber Architecture and Muscle Function." *Exercise and Sport Sciences Reviews* 10: 160–207.

García, L. F., J. C. Valenzuela-Rojas, J. C. González-Gómez, M. Lacava, and A. van der Meijden. 2022. "Pinching or Stinging? Comparing Prey Capture Among Scorpions With Contrasting Morphologies." *Journal of Venomous Animals and Toxins Including Tropical Diseases* 28: 1–9.

Garland, T., and S. C. Adolph. 1994. "Why Not to Do Two-Species Comparative Studies: Limitations on Inferring Adaptation." *Physiological Zoology* 67: 797–828.

Garland, T., C. J. Downs, and A. R. Ives. 2022. "Trade-Offs (and Constraints) in Organismal Biology." *Physiological and Biochemical Zoology* 95: 82–112.

Gilai, A., and I. Parnas. 1970. "Neuromuscular Physiology of the Closer Muscles in the Pedipalp of the Scorpion *Leiurus quinquestriatus*." *Journal of Experimental Biology* 52: 325–344.

Goswami, A., J. B. Smaers, C. Soligo, and P. D. Polly. 2014. "The Macroevolutionary Consequences of Phenotypic Integration: From Development to Deep Time." *Philosophical Transactions of the Royal Society, B: Biological Sciences* 369: 20130254.

Govind, C. K., and F. Lang. 1978. "Development of the Dimorphic Claw Closer Muscles of the Lobster *Homarus americanus*. III. Transformation to Dimorphic Muscles in Juveniles." *Biological Bulletin* 154: 55–67.

Govind, C. K., D. Mellon, and M. M. Quigley. 1987. "Muscle and Muscle Fiber Type Transformation in Clawed Crustaceans." *American Zoologist* 27: 1079–1098.

Govindarajan, S., and G. S. Rajulu. 1974. "Presence of Resilin in a Scorpion *Palamnaeus swammerdami* and Its Role in the Food-Capturing and Sound-Producing Mechanisms." *Experientia* 30: 908–909.

Hedrick, T. L. 2008. "Software Techniques for Two- and Three-Dimensional Kinematic Measurements of Biological and Biomimetic Systems." *Bioinspiration & Biomimetics* 3: 034001.

Herrel, A., J. Podos, B. Vanhooydonck, and A. P. Hendry. 2009. "Force-Velocity Trade-Off in Darwin's Finch Jaw Function: A Biomechanical Basis for Ecological Speciation?" *Functional Ecology* 23: 119–125.

Herrel, A., L. Spithoven, R. Van Damme, and F. DE Vree. 1999. "Sexual Dimorphism of Head Size in Gallotia Galloti: Testing the Niche Divergence Hypothesis by Functional Analyses." *Functional Ecology* 13: 289–297.

Hill, A. V. 1938. "The Heat of Shortening and the Dynamic Constants of Muscle." *Proceedings of the Royal Society of London, Series B, Biological Sciences* 126: 136–195.

Holzman, R., D. C. Collar, S. A. Price, C. D. Hulsey, R. C. Thomson, and P. C. Wainwright. 2012. "Biomechanical Trade-Offs Bias Rates of Evolution in the Feeding Apparatus of Fishes." *Proceedings of the Royal Society B: Biological Sciences* 279: 1287–1292.

Huxley, A. F. 1957. "Muscle Structure and Theories of Contraction." *Progress in Biophysics and Biophysical Chemistry* 7: 255–318.

Labonte, D. 2023. "A Theory of Physiological Similarity in Muscle-Driven Motion." *Proceedings of the National Academy of Sciences* 120: 1–11.

Lee, S. S. M., and S. J. Piazza. 2009. "Built for Speed: Musculoskeletal Structure and Sprinting Ability." *Journal of Experimental Biology* 212: 3700–3707.

Lieber, R. L., B. Ljung, and J. Fridén. 1997. "Intraoperative Sarcomere Length Measurements Reveal Differential Design of Human Wrist Extensor Muscles." *Journal of Experimental Biology* 200: 19–25.

Lieber, R. L., and S. R. Ward. 2011. "Skeletal Muscle Design to Meet Functional Demands." *Philosophical Transactions of the Royal Society, B: Biological Sciences* 366: 1466–1476.

Maganaris, C. N., V. Baltzopoulos, and D. Tsaopoulos. 2006. "Muscle Fibre Length-to-Moment Arm Ratios in the Human Lower Limb Determined In Vivo." *Journal of Biomechanics* 39: 1663–1668.

Martin, M. L., K. J. Travouillon, P. A. Fleming, and N. M. Warburton. 2020. "Review of the Methods Used for Calculating Physiological Cross-Sectional Area (PCSA) for Ecological Questions." *Journal of Morphology* 281: 778–789.

McHenry, M. J. 2011a. "There Is No Trade-Off Between Speed and Force in a Dynamic Lever System." *Biology Letters* 7: 384–386.

McHenry, M. J. 2012. "When Skeletons Are Geared for Speed: The Morphology, Biomechanics, and Energetics of Rapid Animal Motion." *Integrative and Comparative Biology* 52: 588–596.

McHenry, M. J., and A. P. Summers. 2011b. "A Force – Speed Trade-Off Is Not Absolute." *Biology Letters* 7: 880–881.

van der Meijden, A., A. Herrel, and A. Summers. 2010. "Comparison of Chela Size and Pincer Force in Scorpions; Getting a First Grip." *Journal of Zoology* 280: 319–325.

van der Meijden, A., T. Kleinteich, and P. Coelho. 2012. "Packing a Pinch: Functional Implications of Chela Shapes in Scorpions Using Finite Element Analysis." *Journal of Anatomy* 220: 423–434.

Nagano, A., and T. Komura. 2003. "Longer Moment Arm Results in Smaller Joint Moment Development, Power and Work Outputs in Fast Motions." *Journal of Biomechanics* 36: 1675–1681.

Osgood, A. C., G. P. Sutton, and M. Cox. 2021. "Simple Muscle-Lever Systems Are Not so Simple: The Need for Dynamic Analyses to Predict Lever Mechanics That Maximize Speed." *Biorxiv*: 1–19. https://doi.org/10.1101/2020.10.14.339390.

Polet, D. T., and D. Labonte. 2024. "Optimal Gearing of Musculoskeletal Systems." *Integrative and Comparative Biology* 64: 987–1006.

Powell, P. L., R. R. Roy, P. Kanim, M. A. Bello, and V. R. Edgerton. 1984. "Predictability of Skeletal Muscle Tension From Architectural Determinations in Guinea Pig Hindlimbs." *Journal of Applied Physiology* 57: 1715–1721.

Püffel, F., R. Johnston, and D. Labonte. 2023. "A General Biomechanical Model for the Relation Between Bite Force and Mandibular Opening Angle in Arthropods." *Royal Society Open Science* 10: 1–22.

R Development Core Team. 2022. R: A Language and Environment for Statistical Computing. R Foundation for Statistical Computing. https://www.R-project.org.

Rik. 2022. Point to Line Distance. https://github.com/thrynae/point_to_line_distance/releases/tag/1.3.2.

Rospars, J. P., and N. Meyer-Vernet. 2016. "Force Per Cross-Sectional Area From Molecules to Muscles: A General Property of Biological Motors." *Royal Society Open Science* 3: 160313.

Sansalone, G., S. Wroe, G. Coates, M. R. G. Attard, and C. Fruciano. 2024. "Unexpectedly Uneven Distribution of Functional Trade-Offs Explains Cranial Morphological Diversity in Carnivores." *Nature Communications* 15: 3275.

Schelp, M. I., and E. D. Burress. 2025. "Biomechanical Specialization Acts as an Asymmetrical Constraint on the Phenotype." *Integrative Organismal Biology* 7, no. 1: obaf013. https://doi.org/10.1093/iob/obaf013.

Schenk, S. C., and P. C. Wainwright. 2001. "Dimorphism and the Functional Basis of Claw Strength in Six Brachyuran Crabs." *Journal of Zoology* 255: 105–119.

Schindelin, J., I. Arganda-Carreras, E. Frise, et al. 2012. "Fiji: An Open-Source Platform for Biological-Image Analysis." *Nature Methods* 9: 676–682.

Schloerke, B., D. Cook, J. Larmarange, et al. 2021. GGally: Extension to "ggplot2." R Package Version 2.1.2. https://CRAN.R-project.org/package=GGally.

Schultze, W. 1927. "Biology of the Large Philippine Forest Scorpion." *Philippine Journal of Science* 32, no. 3: 375–390.

Simone, Y., C. Chaves, A. van der Meijden, and B. Egeter. 2022. "Metabarcoding Analysis of Different Portions of the Digestive Tract of Scorpions (Scorpiones, Arachnida) Following a Controlled Diet Regime Shows Long Prey DNA Half-Life." *Environmental DNA* 4: 1176–1186.

Simone, Y., and A. van der Meijden. 2018. "Fast and Fine Versus Strong and Stout: A Trade-Off Between Chela Closing Force and Speed Across Nine Scorpion Species." *Biological Journal of the Linnean Society* 123: 208–217.

Simone, Y., and A. van der Meijden. 2021. "Armed Stem to Stinger: A Review of the Ecological Roles of Scorpion Weapons." *Journal of Venomous Animals and Toxins Including Tropical Diseases* 27: 1–21.

Smith, N. C., A. M. Wilson, K. J. Jespers, and R. C. Payne. 2006. "Muscle Architecture and Functional Anatomy of the Pelvic Limb of the Ostrich (*Struthio camelus*)." *Journal of Anatomy* 209: 765–779.

Snodgrass, R. E. 1952. *A Textbook of Arthropod Anatomy*. Comstock Publishing Associates.

Stanley. 2022. Compute 3D Rotation Matrix. MATLAB Central File Exchange. https://www.mathworks.com/matlabcentral/fileexchange/23417-compute-3d-rotation-matrix.

Taylor, G. M. 2000. "Maximum Force Production: Why Are Crabs so Strong?" *Proceedings of the Royal Society of London. Series B: Biological Sciences* 267: 1475–1480.

Wainwright, P. C. 2007. "Functional Versus Morphological Diversity in Macroevolution." *Annual Review of Ecology, Evolution, and Systematics* 38: 381–401.

Wakeling, J. M., O. M. Blake, I. Wong, M. Rana, and S. S. M. Lee. 2011. "Movement Mechanics as a Determinate of Muscle Structure, Recruitment and Coordination." *Philosophical Transactions of the Royal Society, B: Biological Sciences* 366: 1554–1564.

Williams, S. B., A. M. Wilson, J. Daynes, K. Peckham, and R. C. Payne. 2008. "Functional Anatomy and Muscle Moment Arms of the Thoracic Limb of an Elite Sprinting Athlete: The Racing Greyhound (*Canis familiaris*)." *Journal of Anatomy* 213: 373–382.

Wolff, J. O., and S. N. Gorb. 2016. "Mechanical Attachment Devices." In *Attachment Structures and Adhesive Secretions in Arachnids*, edited by S. N. Gorb and C. Albrecht, 25–52. Springer.

Supporting Information

Additional supporting information can be found online in the Supporting Information section.